# Product characterization and preclinical evaluation of the biodistribution and safety of umbilical cord mesenchymal stromal cell-derived extracellular vesicles

**Zaquer Suzana Munhoz Costa-Ferro**
IDOR: Instituto D'Or de Pesquisa e Ensino
**Gisele Vieira Rocha**
IDOR: Instituto D'Or de Pesquisa e Ensino
**Kátia Nunes da Silva**
Hospital São Rafael: Hospital Sao Rafael
**Bruno Diaz Paredes**
IDOR: Instituto D'Or de Pesquisa e Ensino
**Erick Correia Loiola**
IDOR: Instituto D'Or de Pesquisa e Ensino
**John Lenon de Souza Santos**
FIOCRUZ Bahia: Instituto Goncalo Moniz
**Rosane Borges Dias**
FIOCRUZ Bahia: Instituto Goncalo Moniz
**Cláudio Pereira Figueira**
FIOCRUZ Bahia: Instituto Goncalo Moniz
**Camila Indiani Oliveira**
FIOCRUZ Bahia: Instituto Goncalo Moniz
**Ludmilla David de Moura**
UNICAMP: Universidade Estadual de Campinas
**Lígia Nunes de Morais Ribeiro**
UNICAMP: Universidade Estadual de Campinas
**Eneida de Paula**
UNICAMP: Universidade Estadual de Campinas
**Dalila Lucíola Zanette**
ICC: Instituto Carlos Chagas
**Clarissa Araújo Gurgel Rocha**
FIOCRUZ Bahia: Instituto Goncalo Moniz
**Patricia Rieken Macedo Rocco**
UFRJ: Universidade Federal do Rio de Janeiro

**Bruno Solano de Freitas Souza** ( bruno.solano@fiocruz.br )
Centro de Pesquisas Goncalo Moniz https://orcid.org/0000-0003-3771-0439

**Research Article**

**Keywords:** mesenchymal stromal cells, extracellular vesicles, proteomics, preclinical, biodistribution, toxicity

**Posted Date:** July 19th, 2023

**DOI:** https://doi.org/10.21203/rs.3.rs-2949774/v1

## Abstract

# Background

Extracellular vesicles (EVs) represent a new axis of intercellular communication that can be explored for therapeutic purposes; they have garnered considerable attention for their potential as cell-free therapy. The clinical application of mesenchymal stromal cell (MSC)-derived EVs is still in its infancy and faces many challenges. The heterogeneity inherent to MSCs, differences among donors, tissue sources, and variations in manufacturing conditions may influence the release of EVs and their cargo, thus potentially affecting the quality and consistency of the final product. We investigated the influence of cell culture and conditioned medium harvesting conditions on the physicochemical and proteomic profile of human umbilical cord MSC-derived EVs (hUCMSC-EVs) produced under current good manufacturing practice (cGMP) standards. We also evaluated the efficiency of the protocol in terms of yield, purity, productivity, and expression of surface markers, and assessed the biodistribution and toxicity of hUCMSC-EVs in preclinical studies.

# Methods

hUCMSCs were isolated from a single cord tissue donor, cultured, cryopreserved, and characterized at a cGMP facility. The conditioned medium was harvested at 24, 48, and 72 h after the addition of EV collection medium. Three conventional methods (nanoparticle tracking analysis, transmission electron microscopy, and nanoflow cytometry) and mass spectrometry were used to characterize the hUCMSC-EVs. Safety (toxicity of single and repeated doses) and biodistribution were evaluated in naive male BALB/c mice (6–8 weeks old) after intravenous administration of the product.

# Results

hUCMSC-EVs were successfully isolated using a cGMP-compliant protocol. Comparison of hUCMSC-EVs purified from multiple harvests revealed progressive EV productivity and slight changes in the proteomic profile, presenting higher homogeneity at later timepoints of conditioned medium harvesting. The comparison of hUCMSC-EVs at 24 and 72 h showed that unique protein-coding gene clusters at 24 h were mainly involved in complement activation, particularly the classic pathway, as well as in innate immune response and positive regulation of B cell activation. The results showed reduced variability of differential proteins and indicated contrasting characteristics (48 versus 72 h). Pooled hUCMSC-EVs showed a non-toxic profile after single and repeated intravenous administration to naive mice.

# Conclusion

hUCMSC-EVs were successfully isolated following a cGMP-compliant protocol, with consistent characteristics and safety profiles, supporting their future clinical development as cell-free therapies.

# Introduction

Mesenchymal stromal cells (MSCs) are multipotent progenitors that can be isolated from different sources, such as bone marrow, adipose tissue, and the umbilical cord [1]. The therapeutic potential of MSCs is related to a plethora of immunomodulatory, anti-inflammatory, and pro-repair effects that are partially mediated by their secretome [1, 2]. Among the components of the MSCs' secretome, extracellular vesicles (EVs) have garnered considerable attention as their therapeutic properties are similar to their parent cells [3, 4].

EVs are surrounded by a bilipid membrane and range in size from 30 to 1,000 nm. Based on their biogenesis, EVs can be classified as exosomes, microvesicles (or ectosomes), and apoptotic bodies [5]. EVs are emerging as novel mediators of intercellular communication under normal and pathological conditions, as they carry several bioactive molecules, including cytosolic and transmembrane proteins, lipids, lipoproteins, integrins, growth factors, enzymes, mRNA, and microRNA (miRNA) [6–9]. Therefore, they play an important role in biomarker discovery and as new therapeutic agents for cell-free therapies [10].

Compared with living cell therapy products, the therapeutic use of EVs offer several advantages, such as lower alloreactivity, less complicated storage conditions, handling, stability, and usage, which ultimately facilitates their distribution and use in the real world [11]. However, the clinical application of MSC-derived EVs (MSC-EVs) is still in its infancy and faces many challenges [12]. As for any medicine, the translational path of such products requires a demonstration of its quality, in-vivo biodistribution, safety, and efficacy [13, 14]. The large-scale production of MSC-EVs under current good manufacturing practice (cGMP) standards, must be implemented and validated for each product. Therefore, many ongoing studies have attempted to standardize the methods of isolation, purification, and characterization of MSC-EVs [15].

Variability in manufacturing conditions, in addition to the inherent heterogeneity of MSCs, may quantitatively and qualitatively influence the release of EVs and their cargo, eventually leading to poor quality and consistency of the final EV product [16]. The similarity between the samples at every multiple-conditioned medium harvest also needs to be evaluated. Therefore, a deeper understanding of the EV biology, cargo, and functions, along with a precise and accurate characterization of MSC-EV-based products and data regarding their systemic distribution and delivery, are necessary to boost the development of such products [2, 17]. We aimed to provide novel insights for future MSC-EV research and treatment selection. We investigated the influence of the culture and harvesting conditions on the EV proteomic profile, productivity, and the expression of surface markers, and evaluated the biodistribution and toxicity in preclinical studies.

## Materials and methods

# Production of human umbilical cord mesenchymal stromal cell-extracellular vesicles

Human umbilical cord MSC-derived EVs (hUCMSCs) were isolated from a single donor's cord tissue, cultured, cryopreserved, and characterized at the cGMP facility of the Center for Biotechnology and Cell Therapy, São Rafael Hospital, Salvador, Brazil. The characterization of hUCMSCs was conducted by flow cytometry, in-vitro trilineage differentiation assay, sterility, and other relevant quality control criteria described previously [18]. hUCMSCs (passage 3) were obtained from the biobank, thawed, and plated in stacks with the CellBind surface (HyperFlask, Corning, NY, USA) and cultured in cGMP xeno-free growth medium (RoosterNourish; RoosterBio, Frederick, MD, USA). The growth medium was removed when 80% confluence was achieved. After washing with Cell Therapy Systems-Dulbecco's phosphate-buffered saline (CTS-DPBS; Thermo Fisher Scientific, Waltham, MA, USA), the EV collection medium was added (Rooster EV Collect, RoosterBio). The medium was harvested at 24, 48, and 72 h after adding the hUCMSC-EV collection medium. Cell count and viability were evaluated by adding acridine orange and propidium iodide (AOPI) fluorescent dye (Logos Biosystems, Anyang, South Korea) to a diluted cell suspension (1:100 in saline), followed by the addition of 10 µL of cell suspension to each well of a 3-channel slide (Logos Biosystems), and measurement in an automatized cell counter LUNA FX7 (Logos Biosystems). The EV-enriched secretome was purified following either a cGMP-compliant protocol (tangential flow filtration using 650 µm and 500 kDa cartridges; Repligen, Waltham, MA) or a research-grade purification protocol, which was utilized for the biodistribution studies (total exosome isolation reagent; Thermo Fisher Scientific).

# Nanoparticle tracking analysis

For nanoparticle tracking analysis (NTA), the hUCMSC-EV suspensions were diluted in phosphate-buffered saline (PBS) and analyzed in terms of the nanoparticle size (nm) and span (cumulative polydispersity index) and nanoparticle concentration (particles/mL), in a NanoSight NS300 instrument (Malvern Instruments, Malvern, UK) equipped with a sample chamber and a green (532 nm) laser. Samples were manually introduced into the chamber through sterile syringes. Three videos of 30 s each were captured, wherein approximately 2,000 tracks were counted in each measurement, run at room temperature (22–24°C), as described previously [19].

# Transmission electron microscopy

The morphology of hUCMSC-EVs was evaluated by transmission electron microscopy (TEM). Ten microliters of each hUCMSC-EV sample were applied to a formvar carbon-coated grid and held for 5 min for adsorption. The grid was dried, 10 µL of aqueous 2% uranyl citrate was added, and the grid was then incubated for 1 min. The excess stain was removed by touching the edge to a sheet of paper filter and allowing the grid to air dry for 24 h. The samples were observed in a JEOL 1230 microscope (JEOL, Tokyo, Japan) at 80 kV.

# Nanoflow cytometry

For immunophenotyping of hUCMSC-EVs, we used a Cytoflex S cytometer (Beckman Coulter, Brea, CA, USA) configured for nanoflow following the equipment manual. After initial noise discrimination and employing the standard setup for nanoparticle size (Gigamix beads; BioCytex, Marseille, France), we selected a sub-population for analysis, whose sizes ranged between 100 and 500 nm. For immunophenotyping, hUCMSC-EVs were stained with CD63-PE (Beckman Coulter), CD81-PE (Invitrogen, Waltham, MA, USA), and CD90-APC (BD Biosciences, Franklin Lakes, NJ, USA). The samples were incubated with the antibodies for 30 min at room temperature and protected from light. Samples were diluted (1:2,000) with the appropriate buffer before acquisition. Data analysis was conducted using the CytExpert v.2.5 software (Beckman Coulter).

# Protein quantification

The total protein concentration was measured according to the manufacturer's instructions, using the reagents in a Qubit protein assay kit (Q33211; Thermo Fisher Scientific). Samples were not diluted and compared with a three-point calibration curve. Ten-microliter samples were combined with 190 µL of the Qubit working solution and measured in duplicates on a Qubit 4 fluorometer (Thermo Fisher Scientific).

# Proteomic analysis

Protein extraction was conducted by incubating samples in a buffer containing 4% sodium dodecyl sulfate (SDS), 0.1 M dithiothreitol (DTT), 0.1 M Tris-HCl (pH 7.5), and protease inhibitors. This solution was pelleted, the supernatant was recovered, and the protein content was quantified using the Qubit protein assay kit in a Qubit fluorometer (Thermo Fisher Scientific). Ten micrograms of the protein lysate were loaded into the denaturing polyacrylamide gel (10% sodium dodecyl-sulfate polyacrylamide gel electrophoresis (SDS-PAGE) solution) and stained with Coomassie blue. Bands were cut from the gel and discolored using a solution of 25 mM ethanol and 50% ammonium bicarbonate (ABC). The gel pieces were dehydrated and dried in a SpeedVac, then reduced (10 mM DTT solution in 50 mM ABC) and alkylated (55 mM iodoacetamide in 50 mM ABC). The liquid portion was discarded, and the fragments were digested with trypsin (50 mmol in ABC buffer) for 20 min at 4°C. The excess trypsin solution was removed, and digestion buffer was added to the fragments and incubated overnight at 37°C. The peptides were extracted twice with acetonitrile under agitation for 10 min at 25°C. The resulting sample was concentrated in a SpeedVac to 10–20% of the original volume. Peptides were purified with StageTips-C18, dried, and placed in a SpeedVac system for 30 min without heating. The sample was diluted in an AD solution (0.1% formic acid, 5% dimethyl sulfoxide, and 5% acetonitrile), for prompt analysis in a gradient for over 60 min by liquid chromatography-tandem mass spectrometry (LC-MS/MS) in an Eksigent NanoLC 1D plus liquid chromatography equipment. The analytical columns measured 15 cm with an internal diameter of 75 µm, containing 3 µm diameter C18 particles (Dr. Maisch, Ammerbuch, Germany). Mass spectrometry was conducted in a hybrid mass spectrometer equipment (LTQ Orbitrap XL ETD; Thermo Scientific). The top 10 most intense ions were fragmented, with CID30 and 30-s dynamic

deletion. The mass spectrometry proteomics data were deposited to the Proteome X change Consortium via the Proteomics Identification (PRIDE) partner repository [20] with the dataset identifier PXD038850.

# Differentially expressed protein analysis

Proteomics statistics were conducted based on label-free quantification (LFQ) of protein abundance processed with the MaxQuant platform. Identified proteins showing a false discovery rate value of ≥ 1% were filtered. The generated “proteinGroups.txt” table was imported into R (version 4.2) to search for differentially expressed proteins.

The R package differential enrichment analysis of proteomics (DEP) data were used to analyze the differentially expressed proteins at 24, 48, and 72 h. The contaminant and reverse proteins were removed. The remaining data were filtered for proteins that showed an LFQ of > 0 in at least one group. The resulting LFQ intensities were normalized, and imputed using random draws from a Gaussian distribution centered around a minimal value ($P < 0.01$). Finally, differential enrichment analysis was conducted in DEP, using the Limma function, selecting proteins with $P$-adjusted and $\log_2$ (fold change) values of < 0.01 and > 1, respectively.

# Protein–protein interaction network analysis

The Search Tool for the Retrieval of Interacting Genes/Proteins (STRING) database (https://string-db.org/) was used to screen protein–protein interaction (PPI) networks with an interaction score of ≥ 0.7. Cytoscape software (version 11.5) was used to illustrate the network. The enrichment analysis Cytoscape plug-in was used to identify significant Gene Ontology (GO) biological processes (BPs) for each network.

# Gene set enrichment analysis

GO and Kyoto Encyclopedia of Genes and Genomes pathway enrichment analyses were conducted using the Database for Annotation, Visualization, and Integrated Discovery (DAVID) (david.ncifcrf.gov). A cut-off criterion was set at $P < 0.01$ to select only significant terms.

# Animals

All experimental animal procedures, and protocols were reviewed and approved by the Committee for the Use and Care of Animals in Research (CEUA) at Gonçalo Moniz Institute (Fiocruz, Bahia) under protocol number CEUA (ID 021-2021); we followed the principles of the Guide for the Care and Use of Laboratory Animals proposed by the National Institute of Health (NIH) and the Animal Research Reporting of In Vivo Experiments (ARRIVE) [21]. Sixty male BALB/c mice (6–8 weeks old, 18–21 g) were randomized into different groups for the subsequent studies. Animals were maintained in a cage (n = 5) with the optimum conditions of (23 ± 2°C, 50–60% RH), and 12-hour light/dark intervals with free access to food (Quinoa, Paraná, Brazil) and water ad libitum. The individuals conducting the experiments were blinded to the group allocation. We made considerable efforts to minimize the misuse and discomfort of the animals.

# In-vivo biodistribution study

After the characterization of hUCMSC-EVs, we conducted in-vivo experiments for the preclinical evaluation of their biodistribution and safety. To evaluate the in-vivo biodistribution of hUCMSC-EVs after systemic administration, we used the lipophilic dye 1,1-dioctadecyl-3,3,3,3-tetramethylindotricarbocyanine iodide (DiR; Invitrogen), which provides an infrared fluorescent signal. DiR-labeled EVs (DiR-hUCMSC-EVs) were intravenously administered into naive mice via the tail vein, followed by euthanasia for ex-vivo fluorescence imaging. hUCMSC-EVs were incubated with 1 mM DiR at room temperature for 30 min before the isolation of hUCMSC-EVs by ultracentrifugation at 100,000 × *g* for 2 h. Subsequently, the hUCMSC-EV pellet was resuspended in PBS, purified, and stored at − 80°C. DiR-hUCMSC-EVs (30 µg protein/100 µL/mouse, n = 5) or PBS solutions (PBS served as the control, 100 µL/mouse, n = 5) were injected into the mice through the tail vein. The mice were euthanized at 1 and 24 h after injection for the subsequent ex-vivo analysis of organs. Images were captured with excitation/emission filters at 710/770 nm, respectively. The fluorescence signals in the tissues were analyzed using the AMI HTX BLI system (Spectral Instruments Imaging, Tucson, AZ, USA).

# In-vivo toxicity study

We evaluated the toxicity of hUCMSC-EVs (30 µg protein/100 µL/mouse, n = 5 per group) at 24 h and 14 days (single intravenous (IV) administration), or after repeated administrations over either 3 or 6 weeks, as follows: hUCMSC-EVs were administered three times a week, the first dose was intravenously injected through the tail vein, and the second and third doses were administered by the intraperitoneal (IP) route for 3 weeks. One final IP dose was administered after 3 and 6 weeks of dosing, and all the mice were euthanized 1 day after the last dose.

Control groups received Plasma-Lyte (control (CTRL), n = 5) under the same conditions. The health status of the animals, including the body weight, visual and behavioral signs of toxicity and mortality, was measured daily. For all groups, blood samples were collected through the submandibular vein for further hemogram, and biochemical analyses to evaluate the renal and hepatic functions, as described previously [22]. For biochemical analysis, the serum was separated by centrifugation at 3,000 × *g* for 5 min to measure the aspartate aminotransferase (AST), alanine aminotransferase (ALT), blood urea nitrogen (BUN), and creatinine (Cr) in a certified laboratory.

The mice were euthanized by cervical dislocation and samples from the lungs, liver, brain, heart, and kidneys were excised and fixed in 10% formaldehyde. Fragments from the spleen were collected for analyses of the immunophenotype of cell sub-populations by flow cytometry, as described in the subsequent section.

# Immunophenotyping of spleen sub-populations

Mouse spleens were gently homogenized, and the homogenate was washed with PBS and centrifuged at 340 × *g* for 10 min at 4°C. The supernatant was discarded and the red blood cell lysing solution (BD Pharmlyse, BD Biosciences) was added to the pellet. The suspension was centrifuged at 340 × *g* for 10 min at 4°C. Samples were resuspended in saline and antibodies for B lymphocytes (CD45+/CD19), T lymphocytes (CD45+/CD3+), and macrophages (CD45+/CD11b+/F4-80+) were added in the appropriate

tubes and incubated for 20 min at room temperature. The following antibodies were utilized: CD45-PE-Cy5, CD19-PE, CD3-FITC, CD11b-FITC, CD11c-PE-Cy7, and F4-80-PE (all of which were obtained from BD Biosciences). Samples were washed with PBS and centrifuged as before. Samples were resuspended in PBS, and data were acquired using a Fortessa cytometer (BD Biosciences). Data analysis was conducted using the FlowJo (v10) software (FlowJo LLC).

# Tissue processing and histology analysis

Macroscopy was conducted by a pathologist, and gross changes (e.g., size, shape, texture, color, etc.) were recorded. Tissues were processed using a graded alcohol series, cleaned in xylene, and embedded in paraffin wax. The tissue was cut into 5 μm thick slices and stained with hematoxylin and eosin. The slides were scanned in an Axio Imager Z2/VSLIDE (Zeiss, Oberkochen, Germany) using 10× and 20× objectives [23]. Histologic findings that were present exclusively in the hUCMSC-EV-treated groups were considered to be treatment-specific.

# Statistical analysis

Different variables were compared using one-way analysis of variance (ANOVA), followed by the Tukey post hoc test. For in-vivo analysis, we conducted Student *t* tests with *P* values adjusted for multiple comparisons ($n = 3$, $\alpha^* = 0.0167$, $\alpha^*$ Bonferroni-adjusted test). We used the Kolmogorov–Smirnov test with Lilliefors correction and Levene's median test to assess the normality and equality of variance, respectively, for all the analysis of variance residuals, wherein all *P* values were ≥ 0.17. Parametric data are expressed as means (standard deviation). All tests were conducted using GraphPad Prism version 9.1.1. (La Jolla, CA, USA). *P* values of < 0.05 were considered to be significant. A Venn diagram was created in the R environment with the Venn diagram package.

## Results

# Characterization of hUCMSC-EVs

We evaluated the physicochemical properties of hUCMSC-EVs obtained at different harvesting times (24, 48, and 72 h) by basic characterization using three conventional methods (TEM, NTA, and nanoflow cytometry). In all samples, TEM analysis revealed the presence of hUCMSC-EVs surrounded by membranes with typical cup-like morphology and average sizes of < 200 nm (Fig. 1A). Nanoparticle size distribution curves showed particles with sizes of < 500 nm (Fig. 1B). The mean sizes of the nanoparticles were 191.2 ± 6.6, 170.3 ± 10.0, and 168.0 ± 9.9 nm after 24, 48, and 72 h, respectively, demonstrating that the size ($P = 0.037$) at 72 h was significantly reduced when compared with the size at 24 h (Fig. 1C). The nanoparticle concentrations increased progressively from $2.63 \pm 0.25 \times 10^9$ and $4.52 \pm 0.48 \times 10^9$ particles/mL at 24 and 48 h ($P < 0.001$ versus 24 h), respectively, to $5.31 \pm 0.40 \times 10^9$ particles/mL at 72 h ($P < 0.0001$ versus 24 h) (Fig. 1D). The purity of the hUCMSC-EV preparations, measured as the ratio between the EV and the protein concentrations, also progressively increased with time ($7.2 \pm 1.0 \times 10^9$, $14 \pm 2.9 \times 10^9$, and $26 \pm 12.0 \times 10^9$ particles/μg at 24, 48, and 72 h, respectively)

(Fig. 1E). The productivity of hUCMSC-EVs at all timepoints showed no significant changes (12 ± 1.7 × $10^3$, 21 ± 4.5 × $10^3$, and 25 ± 11.0 × $10^3$ particles/cell at 24, 48, and 72 h, respectively) (Fig. 1F). The cells showed high viability (86 ± 13%) 72 h after the addition of the EV collection medium, suggesting that the culture conditions had a minor impact on cell viability.

Nanoflow cytometry analysis was used to provide a quantitative measure of hUCMSC-EV markers (Fig. 2). Analysis of the hUCMSC-EV sub-population between 100 and 500 nm showed the presence, of the tetraspanins CD63 (13.01, 28.6, and 21.1% at 24, 48, and 72 h, respectively); CD81 (21.7, 40.4, and 32.8% at 24, 48, and 72 h, respectively); and CD90 (26.7, 47.3, and 44.0% at 24, 48, and 72 h, respectively) at variable frequencies.

# Analysis of protein content of hUCMSCs and hUCMSC-EVs

hUCMSC-EV samples usually comprise a heterogeneous mixture of small EVs and non-vesicular components [24]. We utilized LC-MS/MS to determine the protein composition of hUCMSC-EV samples obtained at different harvesting times and compared these with the parent cells (hUCMSCs). A total of 1,745 proteins were identified in the proteomic analysis of the parental hUCMSCs, and 718 proteins were detected in hUCMSC-EVs according to UniProt accessions. The proteins quantified in hUCMSCs were compared to those in hUCMSC-EVs, and the results revealed that 470 proteins were shared between the parent cells and their EVs, and 248 were exclusively detected in the hUCMSC-EV samples (Fig. 3A).

The proteins common to the hUCMSC and hUCMSC-EV samples, and those detected exclusively in hUCMSC-EVs were evaluated by GO analysis and summarized by BPs and cellular components. Cellular localization of the proteins shared by hUCMSCs and hUCMSC-EVs showed significant enrichment of 8 cellular compartments, including the cytoplasm, extracellular region, endoplasmic reticulum, endosome, lysosome, vacuole, nucleus, and ribosomes (Fig. 3B). The top 10 BPs associated with the higher number of proteins commonly found in hUCMSCs and hUCMSC-EVs included cell adhesion, protein stabilization, positive regulation of gene expression, and actin cytoskeleton organization (Fig. 3C). The GO analysis conducted against proteins present exclusively in hUCMSC-EV samples showed enriched terms related to the extracellular space, extracellular exosome, cytosol, extracellular matrix structural constituents, and protein binding (Fig. S1). Considering the GO BPs, enriched terms were detected in complement activation, innate immune response, proteolysis, and cell adhesion (Fig. S1).

We identified several proteins from different MISEV2018 categories in the hUCMSC-EV samples: (1) transmembrane or glycosylphosphatidylinositol-anchored proteins associated with the plasma membrane and/or endosomes (i.e. CD63, CD81, CD82, GNAI2, ITGA, ITGB, LAMP1, LAMP2, SDC4, NT5E, HLA-A, CD9, CD90, and CD44); (2) cytosolic proteins recovered in EVs (i.e. ALIX, ANXA*, HSPA8, HSP90AB1, SDCBP, ACTB, and GAPDH); (3) major components of non-EV co-isolated structures (i.e. APOA1, APOA2, and APOB); (4) transmembrane, lipid-bound, and soluble proteins associated with intracellular compartments other than plasma membrane/endosomes (i.e. HIST1H2BC, HIST1H3A,

HIST1H4A, HSPA5, HSP90B1, ACTN1, LMNA, and KRT18); and (5) secreted proteins recovered with EVs (i.e. TGFBI, TGFB2, PDGFC, FN1, and COL*) [7].

# Evaluation of the protein abundance in hUCMSC-EVs and PPI network analysis

The preliminary quantitative analysis of the protein content revealed that 65% of the proteins in the hUCMSC-EVs were compatible with the hUCMSC proteome (Fig. 3A). Comparing the hUCMSC-EV samples from the different harvest timepoints, the assays demonstrated an overlap of 415 proteins (58%), and less than 15% of proteins appeared exclusively at one timepoint, implying a high degree of similarity between the samples (Fig. 4A). To gain further insight into the putative differences between the proteomic profile of hUCMSC-EVs, we investigated the abundance of proteins based on LFQ data according to specific conditions. The expression–abundance curve showed the proteins that have LFQ values greater than zero for at least one condition in each assay. The top 20 gene symbols of loaded proteins were selected for further analysis (Fig. 4B). To investigate the potential functions conducted by top-loaded proteins, the main BPs were evaluated using DAVID (https://david.ncifcrf.gov/). The most significant BP terms in common between the three groups (24, 48, and 72 h) comprised the following: response to mechanical stimulus, collagen fibril organization, extracellular matrix organization, wound healing, angiogenesis, and skin morphogenesis (Fig. 4C). The unique BP terms for assay were highlighted, and hUCMSC-EVs harvested at 24 h showed enriched proteins relating to the integrin-mediated signaling pathway, complement activation, and acute-phase response (Fig. S2). For the 72 h samples, processes associated with cell-matrix adhesion, regulation of NF-kB signaling, and response to cytokines (Fig. S2) were found to be the most significant terms. No unique terms were found for the 48 h samples.

The top-loaded proteins described were compared with proteins contained in EVs according to the Vesiclepedia public database (http://microvesicles.org/). Among the most abundant proteins, fibronectin 1 (FN1), filamin A (FLNA), glyceraldehyde-3-phosphate dehydrogenase (GAPDH), annexin A2 (ANXA2), lectin galactoside-binding soluble 3 binding protein (LGALS3BP; extracellular matrix protein), complement proteins (C3), pyruvate kinase (PKM), actinin alpha 1 (ACTN1; cytoskeletal protein), and elongation factor 1-alpha 1 (EEF1A1; translational factor) are on Vesiclepedia's list of top 100 proteins that are often identified in EVs. According to the GO analysis, these proteins are involved in processes, such as angiogenesis, immune response, response to mechanical stimulus, wound healing, cell differentiation, and response to cytokine cell-matrix adhesion.

To evaluate the interactions between the top-loaded proteins in hUCMSC-EV assays, PPI network analysis was conducted using STRING (version 11.5). A PPI network was constructed for each condition and first-neighbor molecules of the most abundant proteins were detached (Fig. S2). GO indicates several BPs associated with the selected proteins. In this analysis, proteins involved in cell differentiation, angiogenesis, and regulation of inflammatory response were highlighted. Furthermore, the top five proteins with the highest degree of interaction were investigated in all networks (Fig. 5A–C). The results indicated FN1, ACTB, COL1A1, HSP90AA1, EEF1A1, PSMA3, PSMA7, and ITGB1 as hubs, suggesting that

these molecules play a central role in direct (physical), and indirect (functional) associations among the detected proteins. Functional analysis of the proteins contained in the PPI network using STRING demonstrated that the selected hubs were mainly related to the following processes: immune effector, transport, localization, stress response, cellular activation, and response to stimulus (Fig. 5D).

# Differential expression analysis

Differential expression analysis was conducted with hUCMSC-EV proteins from each harvesting time to identify enriched proteins. A volcano plot exhibited higher variability of differential proteins to indicate contrasts: 24 versus 48 h and 24 versus 72 h (fold change > 1.0 and *P* value < 0.05) (Fig. 6A). Heatmap analysis comparing the proteins at 24 and 48 h revealed two main clusters, and the proteins in cluster 1 were related to the innate immune response, positive regulation of B cell activation, phagocytosis, and positive regulation of receptor-mediated endocytosis (Fig. 6B, C). Cluster 2 comprised proteins involved in cellular response to hypoxia, negative regulation of cell population proliferation, negative regulation of mesenchymal cell proliferation, actin cytoskeleton organization, and actin filament network formation according to the UniProt database (https://www.uniprot.org/).

The comparison of proteins between 24 and 72 h showed that unique protein-coding gene clusters at 24 h were mainly involved in complement activation, particularly the classic pathway, as well as innate immune response, and the positive regulation of B cell activation (Fig. 6B, C). These results showed that differential proteins had reduced variability at 48 h compared with those at 72 h, owing to the small rate of differentially expressed proteins among the assays; a complementary proteomics analysis was conducted on a pool of samples collected at different cultivation times. Fifteen of the top 20 most abundant proteins in the pool were also present in the 24-, 48-, and 72 h assays. In addition, these proteins were involved in skin morphogenesis, cellular response to amino acid stimulus, collagen fibril organization, and response to mechanical stimulus (Fig. S3).

# In-vivo biodistribution and toxicity analyses

Considering the high degree of similarity between the hUCMSC-EV samples collected at different timepoints, we used pooled hUCMSC-EVs for in-vivo biodistribution and safety analyses. For the biodistribution analysis, DiR-labeled hUCMSC-EVs were intravenously administered to mice through the tail vein, followed by ex-vivo analysis of different organs (brain, heart, lungs, liver, spleen, and kidneys) after 1 and 24 h (Fig. 7A). We observed a stronger fluorescent signal in the liver compared with that of the control after 1 h of IV administration (Fig. 7E, H). After 24 h, hUCMSC-EVs accumulated in the liver and spleen (Fig. 7E, F, I), showing a non-statistically significant tendency to accumulate in the lungs (Fig. 7C). We did not detect significant fluorescent signals exceeding the control levels in the other evaluated organs (brain, heart, and kidneys; Fig. 7A, D, G).

After the biodistribution evaluation, we investigated the in-vivo safety by analyzing single- and repeated-dose toxicities (Fig. 8A). The body weight of the animals was measured to evaluate the general toxicity

[25] of the hUCMSC-EVs and it did not vary among the groups at the end of the study ($P > 0.05$ for both groups; Fig. 8B–E). The average counts of red blood cells, white blood cells, and platelets were also analyzed. At all timepoints, the mice injected with hUCMSC-EVs, either in a single or multiple doses, showed no significant hematologic changes compared with those in the control group ($P > 0.05$; Fig. 8F, G). The effect of hUCMSC-EVs on liver and kidney function was evaluated by detecting the levels of AST, ALT, BUN, and Cr in the serum of mice. As presented in Tables S1 and S2, no significant differences were observed between the hUCMSC-EV and the control groups ($P > 0.05$). Histopathologic examination did not reveal any significant abnormalities or treatment-related changes in the analyzed heart, kidneys, lungs, spleen, liver, and brain tissues (data not shown).

To assess possible changes in the cellular composition of the spleen related to the immunogenicity, and immunotoxicity we evaluated the frequency of immune cells by flow cytometry (Fig. 9). Flow cytometry analysis of immune sub-populations of the spleen showed no differences in the percentages of macrophages (CD45 + CD11b+/F4-80+) (CTRL, 6.2 ± 3.25%; hUCMSC-EVs, 5.3 ± 1.94%), B lymphocytes (CD45+/CD19+) (CTRL, 66.6 ± 3.53%; hUCMSC-EVs, 64.8 ± 4.68%), and T lymphocytes (CD45+/CD3+) (CTRL, 22.6 ± 1.91%; hUCMSC-EVs, 23.3 ± 3.93%) after 14 days (Fig. 9B). After 3 and 6 weeks (Fig. 9C) of infusion of hUCMSC-EVs, no differences were observed between macrophages, B- and T lymphocytes.

# Discussion

EVs have garnered considerable attention as a mechanism of intercellular communication, and as candidates for therapeutic development as cell-free therapies [26]. In this study, we investigated the potential of hUCMSCs as a source of therapeutic EVs, and provided an in-depth evaluation of the influence of culture and harvest conditions on the final product characteristics, including physical parameters and proteomic profiles.

Compared with other tissue sources of MSCs, hUCMSCs have many advantages, such as the high availability of cord tissue, the high proliferative profile of cells, and their history of successful clinical translation, indicating safety and potential for beneficial therapeutic effects for different diseases [27–29]. As the proof of concept, the safety and potential efficacy of hUCMSCs have been extensively studied in patients with severe Coronavirus disease-19 (COVID-19) in previous studies, including our own work [18, 29, 30]. The same hUCMSCs utilized as the source of EVs in here have been previously utilized to treat a patient with advanced critical COVID-19, showing significant immunomodulatory effects [18]. Thus, we suggest that switching from the therapeutic use of MSCs to their EVs could lead to a superior safety profile, and provide several advantages in terms of logistics, as EV products can be safely stored without significant loss of function; therefore, they can be made available as an off the shelf medicinal product.

A major requirement in the field of therapeutic EVs is the realization of optimal conditions for large-scale manufacturing with high productivity and product lot-to-lot consistency [31]. The use of repeated harvesting protocols is highly desirable to enhance the yield of EVs manufactured in each lot.

Considering the possible variability related to the culture harvesting time in the characteristics of the purified EVs, we compared the characteristics of the EVs obtained 24, 48, and 72 h after the introduction of the EV collection medium. The harvest points studied here are within the range reported in the literature, usually comprising different intervals ranging from 12 h to 7 days [32]. The harvesting time is also influenced by the cell seeding density and prolonged culturing under starvation conditions, which could lead to the loss of viability and an increase in apoptotic bodies during EV preparation. Using the protocol, we depicted consistent production of hUCMSC-EVs for 72 h, with a progressive increase in productivity and yield, while also maintaining cell viability. Similar results regarding the EV productivity have recently been reported by others using different cell sources [33].

Regardless of the harvesting timepoints, the data indicate that hUCMSC-EVs were successfully isolated from hUCMSCs and met the minimum criteria to be classified as EVs [7]. hUCMSC-EVs showed a rounded cup-like morphology with an average diameter of < 200 nm at all evaluated timepoints; however, reduced diameters of hUCMSC-EVs were observed at 48 and 72 h compared with those at 24 h. Immunophenotyping and proteomics showed positive expression of tetraspanins (CD63, CD9, CD81, and CD82) and markers of the origin of MSCs (CD44 and CD90), independent of the harvesting time [33, 34]. Proteomic data of hUCMSC-EVs revealed a small set of differentially expressed proteins at 24 h compared with that at 48 h and 72 h, which were remarkably similar. Two clusters of proteins enriched at 24 h were related to phagocytosis, positive regulation of B cell activation, innate immune response, and complement activation. The possible influence of these small differences on the safety, and therapeutic profile were not evaluated as we decided to pool the different harvests as recommended by the EVOLVE guidelines for the preclinical biodistribution and safety analyses [35].

The analysis of proteomic data in hUCMSC-EVs indicated the presence of proteins involved in multiple cellular pathways relevant to health and disease. The GO analysis revealed that most proteins found in hUCMSC-EVs were components of the EVs, plasma membrane, cytoplasm, lysosomes, ribosomes, and cytoskeleton, and were involved in signal transduction, energy metabolism, innate immune response, and several other BPs. The analysis of bioinformatic data identified the abundance of proteins that are involved in several processes, such as angiogenesis, immune response, response to mechanical stimulus, wound healing, cell differentiation, and response to cytokine cell-matrix adhesion. Fibronectin 1 (FN1) facilitates cell migration through tissues [36], and exosomal FN1 mediates the mitogenic activity of MSC-derived exosomes [37]. The main components of the glycolytic pathways, GAPDH and PKM, which are known to be exported by EVs, were also present, and are listed among the 10 most frequently identified proteins in EVs (http://microvesicles.org/) [24]. ANXA2 is a protein present in the cell composition of the membrane, extracellular exosome, and EVs. It is involved in many cellular processes, including membrane trafficking events [38]. The involvement of ANXA2 in the loading of RNA into exosomes has been experimentally demonstrated [39]. The extracellular matrix protein, LGALS3BP, is known to interact with a set of membrane molecules, such as integrins, fibronectin, laminins, collagen, nidogen, and galectins [39]. Traditional complement proteins, such as C3, are an important component of the innate immune system, as complement activation results in the generation of activated protein fragments that play a role in inflammatory reactions, immune complex clearance, and antibody production [40]. Structural and

cytoskeletal proteins ACTN1, filamins, such as filamin A, which act as scaffolds for various signaling molecules implicated in cell motility, transcription[41], and mechanical sensing, as well as the most abundant translational factor EEF1A1, which regulates the synthesis of proteins, translation machines, cell proliferation, and apoptosis, were also present in the sample [42, 43].

By analyzing protein associations, we identified 8 hubs comprising these proteins (e.g., FN1 and EEF1A1) and ACTB, COL1A1, HSP90AA1, PSMA3, PSMA7, and ITGB. β-Actin is a major cytoskeletal filament protein encoded by the actin beta (ACTB) gene, and is an important player in cell motility, migration, and gene expression [44]. Molecular chaperones, especially Hsp90, are an evolutionarily conserved class of proteins that assist normal folding, intracellular protein disposition, and proteolytic turnover of the key regulators of cell growth [45]. Lauwers et al. [46] demonstrated that Hsp90 facilitates the transport of multivesicular bodies toward the plasma membrane and enhances exosome secretion. PSMA3 and PSMA7 are proteasome subunits that belong to the 26S proteasome complex. This protease complex is part of the ubiquitin proteasome system, that is the principal proteolytic system responsible for the functional modification and degradation of cellular proteins and processes such as proliferation, growth, differentiation, gene transcription, signaling, and apoptosis [47, 48]. Proteasomes are also present and active in the extracellular compartments, including EVs [49]. Integrin subunit beta 1 (ITGB1) adheres to collagens, laminins, fibronectin, and other glycoproteins. Notably, ITGB1 plays a role in cell adhesion, cell-matrix adhesion and is abundant in exosomes with different origins [50]. These hub proteins are associated with effector immune mechanisms, transport, localization, stress response, cellular activation, and response to stimulus.

The proteomic analysis identified proteins that have previously been enriched in both small EVs (e.g., CD9, CD81, CD63, annexins, ALIX, and aldolase A) and the non-vesicular fractions (GAPDH, PKM, HSP90, EEF2, PGK1, and clathrin) [24]. Although a significant overlap of protein content has been reported in small EVs and non-vesicle fractions, the results suggest that our samples included a mixture of small EVs and non-vesicle components, which is expected for the protocols of isolation and purification used here. Furthermore, a mixture of exosomes and small microvesicles (CD81+/CD63+/CD9+, and annexin A1+) can be expected based on the analysis of protein content [24]. The nanoflow analysis presented here supports the frequency of classic exosomes estimated in approximately 20–30% of the EVs in the preparations. Quantitatively monitoring the frequency of exosome marker expression in each batch, rather than qualitative measurements, may be important to ensure the lot-to-lot consistency [24, 35].

Despite the increasing interest and the developments in the field of therapeutic EVs, only few studies have evaluated the biodistribution of EVs in-vivo, which is a critical step in preclinical development [51]. Our results demonstrated that when intravenously administered to naive mice, hUCMSC-EVs accumulated largely in the liver, spleen, and lungs, which is consistent with previous observations [52]. The identification of EVs in other organs and tissues has also been reported in protocols using higher doses, which could be related to the sensitivity of the methods [53]. EVs injected intravenously have been reported to be cleared by the reticuloendothelial system, and may influence the local or systemic processes of injury and inflammation [54]. Whether this mechanism of clearance by innate immune cells

could be a part of the mechanisms of immune regulation promoted by MSC-EVs still requires further investigation.

In this study, the preclinical toxicology of hUCMSC-EVs was analyzed to identify possible adverse effects. Our results indicate that hUCMSC-EVs are safe in terms of the immune response and toxicity, after either a single systemic IV dose or even after 3- and 6 weeks-long repeated administrations of hUCMSC-EVs. This result is consistent with previous reports, including a study wherein the repeated administration of hUCMSC-EVs showed no signs of immunogenicity [25]. Previous studies evaluating the toxicity of EVs from different sources corroborate our data, demonstrating their safety after IV administration in a single dose or in repeated administrations, even at extremely high doses, such as $2 \times 10^{12}$ EVs/200 µL/mouse, with no reports of acute or subacute toxicities in immunocompetent mice. Thus, through feasible doses, it is not possible to determine the level where adverse effects were observed [55–57]. This emphasized the increased safety profile of EVs compared with MSCs, for which the maximum tolerated dose has been demonstrated, which is related to their pro-thromboembolic activity at high doses [58].

Immune toxicity may occur with biological medicines (e.g., monoclonal antibodies and advanced therapy products), and must therefore be evaluated as part of the preclinical toxicity evaluation of EV products, especially considering that EVs target immune cells as part of their mechanism of action [59, 60]. Our data show that no significant differences were observed between the groups (Plasma-Lyte and hUCMSC-EVs) for any of the tested immune cell populations, indicating that treatment with hUCMSC-EVs did not alter the composition of the immune cells in the spleen. Our results are in accordance with a previous study that demonstrated neither toxicity nor induction of an immune response in immunocompetent mice after repeated administrations of HEK293-derived EVs [61]. Our biodistribution data show that circulating hUCMSC-EVs were present in the spleen 24 h after IV administration. These interactions with distinct spleen cell populations were expected to trigger differential physiological responses and alter local signaling at the autocrine and paracrine levels.

# Conclusion

HUCMSC-EVs were successfully isolated using a cGMP-compliant protocol. The comparison of hUCMSC-EVs purified from multiple harvests revealed progressive EV productivity and slight changes in the proteomic profile, which showed higher homogeneity at later timepoints after the introduction of the EV collection medium. Our results demonstrated the viability of the isolation of clinical-grade hUCMSC-EVs with consistent characteristics, and safety profiles for future clinical development of cell-free therapies.

# Abbreviations

ALT Alanine aminotransferase

ANOVA Analysis of variance

AST Aspartate aminotransferase

| | |
|---|---|
| BP | Biological process |
| BUN | Blood urea nitrogen |
| cGMP | Current good manufacturing practice |
| Cr | Creatinine |
| CTRL | Control group |
| DAVID | Database for Annotation, Visualization, and Integrated Discovery |
| DEP | Differential enrichment analysis of proteomics |
| DiR | 1,1-Dioctadecyl-3,3,3,3-tetramethylindotricarbocyanine iodide |
| EVs | Extracellular vesicles |
| GAPDH | Glyceraldehyde-3-phosphate dehydrogenase |
| GO | Gene Ontology |
| hUCMSC-EVs | Human umbilical cord MSC-derived EVs |
| i.v. | intravenous |
| i.p. | intraperitoneal |
| LC-MS/MS | Liquid chromatography-tandem mass spectrometry |
| LFQ | Label-free quantification |
| MCH | Mean corpuscular hemoglobin |
| MCHC | Mean corpuscular hemoglobin concentration |
| MCV | Mean corpuscular volume |
| MSC | Mesenchymal stromal cell |
| NTA | Nanoparticle tracking analysis |
| PBS | Phosphate-buffered saline |
| PKM | Pyruvate kinase |
| PPI | Protein–protein interaction |

| | |
|---|---|
| RBC | Red blood cell |
| SDS | sodium dodecyl sulfate |
| TEM | Transmission electron microscopy |

# Declarations

Ethics approval and consent to participate

This study was approved by the Committee for the Use and Care of Animals in Research (CEUA) of the Animal Science of the Instituto Gonçalo Moniz (Fiocruz Bahia) under protocol number CEUA ID 021-2021. The production and characterization of hUCMSC-EVs from donor tissue was approved by the National Committee for Ethics in Research (CONEP, CAAE: 30724020.3.1001.0008). All participants gave written informed consent to participate.

Consent for publication

Not applicable.

Availability of data and materials

Data are available via ProteomeXchange with identifier PXD038850 (https://proteomecentral.proteomexchange.org/cgi/GetDataset?ID=PXD038850).

For review purpose only,

Please use : https://www.ebi.ac.uk/pride/archive/projects/PXD038850/private

Submission details:

Project Name: PRODUCT CHARACTERIZATION AND PRECLINICAL SAFETY OF

UMBILICAL CORD MESENCHYMAL STROMAL CELL-DERIVED SMALL

EXTRACELLULAR VESICLES

Project accession: PXD038850

Project DOI: Not applicable

Username: reviewer_pxd038850@ebi.ac.uk

Password: QkzXYp10

Competing interests

The authors declare that they have no competing interests.

Funding

This paper was funded by the Brazilian Council for Scientific and Technological Development (CNPq), the Rio de Janeiro State Research Foundation (FAPERJ), the Department of Science and Technology (DECIT)/Brazilian Ministry of Health, the Coordination for the Improvement of Higher Education Personnel (CAPES), National Institute of Science and Technology for Regenerative Medicine, D'OR Institute Research & Education, and Maria Emilia Foundation. Funding organizations played no role in the design or conduct of the study, data interpretation, or writing of the article. Patricia R.M. Rocco (Research Productivity, PQ1A), Bruno Solano de Freitas Souza, Clarissa Araújo Gurgel Rocha (Research Productivity, PQ2) and Camila Indiani de Oliveira (Research Productivity, PQ1C) are supported by CNPq.

Authors' contributions

ZSMCF designed the study, performed *in vivo* experiments, analyses, and wrote the manuscript. GVR performed the bioinformatic analyses. KNS, BDP, and ECL performed cell cultures and EV purification, flow cytometry, and protein analyses. JLSS and DLZ performed the mass spectrometry experiments. CPF performed the electron microscopy analyses. RBD and CAGR performed histologic processing and analyses. CIO performed spleen immunophenotyping analyses. LDM, LNMR, and EP performed the NTA analyses. PRMR and BSFS designed the study, provided funding, as well as wrote and reviewed the manuscript. All authors read and approved the final manuscript.

Acknowledgments

The authors would like to thank Ms. Roquelina Assis for technical support.

# References

1. Margiana R, Markov A, Zekiy AO, Hamza MU, Al-Dabbagh KA, Al-Zubaidi SH et al. Clinical application of mesenchymal stem cell in regenerative medicine: a narrative review. Stem Cell Res Ther [Internet]. 20220728th ed. 2022;13:366. Available from: https://www.ncbi.nlm.nih.gov/pubmed/35902958.
2. da Silva KN, Gobatto ALN, Costa-Ferro ZSM, Cavalcante BRR, Caria ACI, de Aragão França LS et al. Is there a place for mesenchymal stromal cell-based therapies in the therapeutic armamentarium against COVID-19? Stem Cell Res Ther [Internet]. 20210727th ed. 2021;12:425. Available from: https://www.ncbi.nlm.nih.gov/pubmed/34315546.
3. Dong B, Wang C, Zhang J, Gu Y, Guo X, Zuo X et al. Exosomes from human umbilical cord mesenchymal stem cells attenuate the inflammation of severe steroid-resistant asthma by reshaping macrophage polarization. Stem Cell Res Ther [Internet]. 20210324th ed. 2021;12:204. Available from: https://www.ncbi.nlm.nih.gov/pubmed/33761997.
4. Thomi G, Surbek D, Haesler V, Joerger-Messerli M, Schoeberlein A. Exosomes derived from umbilical cord mesenchymal stem cells reduce microglia-mediated neuroinflammation in perinatal brain injury.

Stem Cell Res Ther [Internet]. 20190321st ed. 2019;10:105. Available from: https://www.ncbi.nlm.nih.gov/pubmed/30898154.

5. Jafarinia M, Alsahebfosoul F, Salehi H, Eskandari N, Ganjalikhani-Hakemi M. Mesenchymal Stem Cell-Derived Extracellular Vesicles: A Novel Cell-Free Therapy. Immunol Invest [Internet]. 20200202nd ed. 2020;49:758–80. Available from: https://www.ncbi.nlm.nih.gov/pubmed/32009478.
6. Dabrowska S, Andrzejewska A, Janowski M, Lukomska B. Immunomodulatory and Regenerative Effects of Mesenchymal Stem Cells and Extracellular Vesicles: Therapeutic Outlook for Inflammatory and Degenerative Diseases. Front Immunol [Internet]. 20210205th ed. 2020;11:591065. Available from: https://www.ncbi.nlm.nih.gov/pubmed/33613514.
7. Théry C, Witwer KW, Aikawa E, Alcaraz MJ, Anderson JD, Andriantsitohaina R et al. Minimal information for studies of extracellular vesicles 2018 (MISEV2018): a position statement of the International Society for Extracellular Vesicles and update of the MISEV2014 guidelines. J Extracell Vesicles [Internet]. 20181123rd ed. 2018;7:1535750. Available from: https://www.ncbi.nlm.nih.gov/pubmed/30637094.
8. Maas SLN, Breakefield XO, Weaver AM. Extracellular Vesicles: Unique Intercellular Delivery Vehicles. Trends Cell Biol [Internet]. 20161213th ed. 2017;27:172–88. Available from: https://www.ncbi.nlm.nih.gov/pubmed/27979573.
9. van der Pol E, Böing AN, Gool EL, Nieuwland R. Recent developments in the nomenclature, presence, isolation, detection and clinical impact of extracellular vesicles. J Thromb Haemost [Internet]. 20151229th ed. 2016;14:48–56. Available from: https://www.ncbi.nlm.nih.gov/pubmed/26564379.
10. Agrahari V, Burnouf PA, Chew CH, Burnouf T. Extracellular Microvesicles as New Industrial Therapeutic Frontiers. Trends Biotechnol [Internet]. 20190109th ed. 2019;37:707–29. Available from: https://www.ncbi.nlm.nih.gov/pubmed/30638682.
11. Yáñez-Mó M, Siljander PR, Andreu Z, Zavec AB, Borràs FE, Buzas EI et al. Biological properties of extracellular vesicles and their physiological functions. J Extracell Vesicles [Internet]. 20150514th ed. 2015;4:27066. Available from: https://www.ncbi.nlm.nih.gov/pubmed/25979354.
12. Massa M, Croce S, Campanelli R, Abbà C, Lenta E, Valsecchi C et al. Clinical Applications of Mesenchymal Stem/Stromal Cell Derived Extracellular Vesicles: Therapeutic Potential of an Acellular Product. Diagnostics (Basel) [Internet]. 20201124th ed. 2020;10. Available from: https://www.ncbi.nlm.nih.gov/pubmed/33255416.
13. Salvadori M, Cesari N, Murgia A, Puccini P, Riccardi B, Dominici M. Dissecting the Pharmacodynamics and Pharmacokinetics of MSCs to Overcome Limitations in Their Clinical Translation. Mol Ther Methods Clin Dev [Internet]. 20190517th ed. 2019;14:1–15. Available from: https://www.ncbi.nlm.nih.gov/pubmed/31236426.
14. Krampera M, Le Blanc K. Mesenchymal stromal cells: Putative microenvironmental modulators become cell therapy. Cell Stem Cell [Internet]. 2021;28:1708–25. Available from: https://www.ncbi.nlm.nih.gov/pubmed/34624232.

15. Varderidou-Minasian S, Lorenowicz MJ. Mesenchymal stromal/stem cell-derived extracellular vesicles in tissue repair: challenges and opportunities. Theranostics [Internet]. 20200501st ed. 2020;10:5979–97. Available from: https://www.ncbi.nlm.nih.gov/pubmed/32483432.
16. Fernández-Santos ME, Garcia-Arranz M, Andreu EJ, García-Hernández AM, López-Parra M, Villarón E et al. Optimization of Mesenchymal Stromal Cell (MSC) Manufacturing Processes for a Better Therapeutic Outcome. Front Immunol [Internet]. 20220609th ed. 2022;13:918565. Available from: https://www.ncbi.nlm.nih.gov/pubmed/35812460.
17. Almeria C, Kreß S, Weber V, Egger D, Kasper C. Heterogeneity of mesenchymal stem cell-derived extracellular vesicles is highly impacted by the tissue/cell source and culture conditions. Cell Biosci [Internet]. 20220502nd ed. 2022;12:51. Available from: https://www.ncbi.nlm.nih.gov/pubmed/35501833.
18. da Silva KN, Pinheiro PCG, Gobatto ALN, Passos RDH, Paredes BD, França LSA et al. Immunomodulatory and Anti-fibrotic Effects Following the Infusion of Umbilical Cord Mesenchymal Stromal Cells in a Critically Ill Patient With COVID-19 Presenting Lung Fibrosis: A Case Report. Front Med (Lausanne) [Internet]. 20211117th ed. 2021;8:767291. Available from: https://www.ncbi.nlm.nih.gov/pubmed/34869480.
19. Ribeiro LNM, Couto VM, Fraceto LF, de Paula E. Use of nanoparticle concentration as a tool to understand the structural properties of colloids. Sci Rep [Internet]. 20180117th ed. 2018;8:982. Available from: https://www.ncbi.nlm.nih.gov/pubmed/29343691.
20. Perez-Riverol Y, Bai J, Bandla C, García-Seisdedos D, Hewapathirana S, Kamatchinathan S et al. The PRIDE database resources in 2022: a hub for mass spectrometry-based proteomics evidences. Nucleic Acids Res [Internet]. 2022;50:D543–52. Available from: https://www.ncbi.nlm.nih.gov/pubmed/34723319.
21. Kilkenny C, Browne WJ, Cuthill IC, Emerson M, Altman DG. Improving bioscience research reporting: the ARRIVE guidelines for reporting animal research. PLoS Biol [Internet]. 20100629th ed. 2010;8:e1000412. Available from: https://www.ncbi.nlm.nih.gov/pubmed/20613859.
22. Golde WT, Gollobin P, Rodriguez LL. A rapid, simple, and humane method for submandibular bleeding of mice using a lancet. Lab Anim (NY) [Internet]. 2005;34:39–43. Available from: https://www.ncbi.nlm.nih.gov/pubmed/16195737.
23. Maronpot RR, Boorman GA, Gaul BW. Pathology of the mouse: reference and atlas. Vienna, IL: Cache River Press; 1999.
24. Jeppesen DK, Fenix AM, Franklin JL, Higginbotham JN, Zhang Q, Zimmerman LJ et al. Reassessment of Exosome Composition. Cell [Internet]. 2019;177:428–445.e18. Available from: https://www.ncbi.nlm.nih.gov/pubmed/30951670.
25. Rodrigues SC, Cardoso RMS, Gomes CF, Duarte FV, Freire PC, Neves R et al. Toxicological Profile of Umbilical Cord Blood-Derived Small Extracellular Vesicles. Membranes (Basel) [Internet]. 20210824th ed. 2021;11. Available from: https://www.ncbi.nlm.nih.gov/pubmed/34564463.

26. Pegtel DM, Gould SJ, Exosomes. Annu Rev Biochem [Internet]. 2019;88:487–514. Available from: https://www.ncbi.nlm.nih.gov/pubmed/31220978.
27. Ahn H, Lee SY, Jung WJ, Lee KH. Treatment of acute ischemic stroke by minimally manipulated umbilical cord-derived mesenchymal stem cells transplantation: A case report. World J Stem Cells [Internet]. 2021;13:1151–9. Available from: https://www.ncbi.nlm.nih.gov/pubmed/34567432.
28. Xie Q, Liu R, Jiang J, Peng J, Yang C, Zhang W et al. What is the impact of human umbilical cord mesenchymal stem cell transplantation on clinical treatment? Stem Cell Res Ther [Internet]. 20201201st ed. 2020;11:519. Available from: https://www.ncbi.nlm.nih.gov/pubmed/33261658.
29. Can A, Celikkan FT, Cinar O. Umbilical cord mesenchymal stromal cell transplantations: A systemic analysis of clinical trials. Cytotherapy [Internet]. 20170928th ed. 2017;19:1351–82. Available from: https://www.ncbi.nlm.nih.gov/pubmed/28964742.
30. Yang CW, Chen RD, Zhu QR, Han SJ, Kuang MJ. Efficacy of umbilical cord mesenchymal stromal cells for COVID-19: A systematic review and meta-analysis. Front Immunol [Internet]. 20220829th ed. 2022;13:923286. Available from: https://www.ncbi.nlm.nih.gov/pubmed/36105796.
31. Adlerz K, Patel D, Rowley J, Ng K, Ahsan T. Strategies for scalable manufacturing and translation of MSC-derived extracellular vesicles. Stem Cell Res [Internet]. 20200902nd ed. 2020;48:101978. Available from: https://www.ncbi.nlm.nih.gov/pubmed/32947235.
32. Rayamajhi S, Sulthana S, Ferrel C, Shrestha TB, Aryal S. Extracellular vesicles production and proteomic cargo varies with incubation time and temperature. Exp Cell Res [Internet]. 20221227th ed. 2023;422:113454. Available from: https://www.ncbi.nlm.nih.gov/pubmed/36584743.
33. Ramos L, Sánchez-Abarca T, Muntión LI, Preciado S, Puig S, López-Ruano N et al. G,. MSC surface markers (CD44, CD73, and CD90) can identify human MSC-derived extracellular vesicles by conventional flow cytometry. Cell Commun Signal [Internet]. 20160112th ed. 2016;14:2. Available from: https://www.ncbi.nlm.nih.gov/pubmed/26754424.
34. Romanov YA, Volgina NE, Dugina TN, Kabaeva NV, Sukhikh GT. Human Umbilical Cord Mesenchymal Stromal Cell-Derived Microvesicles Express Surface Markers Identical to the Phenotype of Parental Cells. Bull Exp Biol Med [Internet]. 20181112th ed. 2018;166:124–9. Available from: https://www.ncbi.nlm.nih.gov/pubmed/30417293.
35. Silva AKA, Morille M, Piffoux M, Arumugam S, Mauduit P, Larghero J et al. Development of extracellular vesicle-based medicinal products: A position paper of the group “Extracellular Vesicle translatiOn to clinicaL perspectiVEs - EVOLVE France.” Adv Drug Deliv Rev [Internet]. 20211019th ed. 2021;179:114001. Available from: https://www.ncbi.nlm.nih.gov/pubmed/34673131.
36. Sung BH, Ketova T, Hoshino D, Zijlstra A, Weaver AM. Directional cell movement through tissues is controlled by exosome secretion. Nat Commun [Internet]. 20150513th ed. 2015;6:7164. Available from: https://www.ncbi.nlm.nih.gov/pubmed/25968605.
37. Yuan O, Lin C, Wagner J, Archard JA, Deng P, Halmai J et al. Exosomes Derived from Human Primed Mesenchymal Stem Cells Induce Mitosis and Potentiate Growth Factor Secretion. Stem Cells Dev

[Internet]. 20190226th ed. 2019;28:398–409. Available from: https://www.ncbi.nlm.nih.gov/pubmed/30638129.

38. Popa SJ, Stewart SE, Moreau K. Unconventional secretion of annexins and galectins. Semin Cell Dev Biol [Internet]. 20180309th ed. 2018;83:42–50. Available from: https://www.ncbi.nlm.nih.gov/pubmed/29501720.
39. Hagiwara K, Katsuda T, Gailhouste L, Kosaka N, Ochiya T. Commitment of Annexin A2 in recruitment of microRNAs into extracellular vesicles. FEBS Lett [Internet]. 20151126th ed. 2015;589:4071–8. Available from: https://www.ncbi.nlm.nih.gov/pubmed/26632510.
40. Holland MC, Lambris JD. The complement system in teleosts. Fish Shellfish Immunol [Internet]. 2002;12:399–420. Available from: https://www.ncbi.nlm.nih.gov/pubmed/12194452.
41. Lamsoul I, Dupré L, Lutz PG. Molecular Tuning of Filamin A Activities in the Context of Adhesion and Migration. Front Cell Dev Biol [Internet]. 20201120th ed. 2020;8:591323. Available from: https://www.ncbi.nlm.nih.gov/pubmed/33330471.
42. Caraglia M, Budillon A, Vitale G, Lupoli G, Tagliaferri P, Abbruzzese A. Modulation of molecular mechanisms involved in protein synthesis machinery as a new tool for the control of cell proliferation. Eur J Biochem [Internet]. 2000;267:3919–36. Available from: https://www.ncbi.nlm.nih.gov/pubmed/10866791.
43. Nilsson J, Nissen P. Elongation factors on the ribosome. Curr Opin Struct Biol [Internet]. 2005;15:349–54. Available from: https://www.ncbi.nlm.nih.gov/pubmed/15922593.
44. Bunnell TM, Burbach BJ, Shimizu Y, Ervasti JM. β-Actin specifically controls cell growth, migration, and the G-actin pool. Mol Biol Cell [Internet]. 20110907th ed. 2011;22:4047–58. Available from: https://www.ncbi.nlm.nih.gov/pubmed/21900491.
45. Picard D. Heat-shock protein 90, a chaperone for folding and regulation. Cell Mol Life Sci [Internet]. 2002;59:1640–8. Available from: https://www.ncbi.nlm.nih.gov/pubmed/12475174.
46. Lauwers E, Wang YC, Gallardo R, Van der Kant R, Michiels E, Swerts J et al. Hsp90 Mediates Membrane Deformation and Exosome Release. Mol Cell [Internet]. 2018;71:689–702.e9. Available from: https://www.ncbi.nlm.nih.gov/pubmed/30193096.
47. Bard JAM, Goodall EA, Greene ER, Jonsson E, Dong KC, Martin A. Structure and Function of the 26S Proteasome. Annu Rev Biochem [Internet]. 20180413th ed. 2018;87:697–724. Available from: https://www.ncbi.nlm.nih.gov/pubmed/29652515.
48. Bhattacharyya S, Yu H, Mim C, Matouschek A. Regulated protein turnover: snapshots of the proteasome in action. Nat Rev Mol Cell Biol [Internet]. 2014;15:122–33. Available from: https://www.ncbi.nlm.nih.gov/pubmed/24452470.
49. Ben-Nissan G, Katzir N, Füzesi-Levi MG, Sharon M. Biology of the Extracellular Proteasome. Biomolecules [Internet]. 20220421st ed. 2022;12. Available from: https://www.ncbi.nlm.nih.gov/pubmed/35625547.
50. Kugeratski FG, Hodge K, Lilla S, McAndrews KM, Zhou X, Hwang RF et al. Quantitative proteomics identifies the core proteome of exosomes with syntenin-1 as the highest abundant protein and a

putative universal biomarker. Nat Cell Biol [Internet]. 20210609th ed. 2021;23:631–41. Available from: https://www.ncbi.nlm.nih.gov/pubmed/34108659.

51. Kang M, Jordan V, Blenkiron C, Chamley LW. Biodistribution of extracellular vesicles following administration into animals: A systematic review. J Extracell Vesicles [Internet]. 20210624th ed. 2021;10:e12085. Available from: https://www.ncbi.nlm.nih.gov/pubmed/34194679.
52. Driedonks T, Jiang L, Carlson B, Han Z, Liu G, Queen SE et al. Pharmacokinetics and biodistribution of extracellular vesicles administered intravenously and intranasally to. J Extracell Biol [Internet]. 20221011th ed. 2022;1. Available from: https://www.ncbi.nlm.nih.gov/pubmed/36591537.
53. Wiklander OP, Nordin JZ, O'Loughlin A, Gustafsson Y, Corso G, Mäger I et al. Extracellular vesicle in vivo biodistribution is determined by cell source, route of administration and targeting. J Extracell Vesicles [Internet]. 20150420th ed. 2015;4:26316. Available from: https://www.ncbi.nlm.nih.gov/pubmed/25899407.
54. Smyth T, Kullberg M, Malik N, Smith-Jones P, Graner MW, Anchordoquy TJ. Biodistribution and delivery efficiency of unmodified tumor-derived exosomes. J Control Release [Internet]. 20141216th ed. 2015;199:145–55. Available from: https://www.ncbi.nlm.nih.gov/pubmed/25523519.
55. Matsuda A, Moirangthem A, Angom RS, Ishiguro K, Driscoll J, Yan IK et al. Safety of bovine milk derived extracellular vesicles used for delivery of RNA therapeutics in zebrafish and mice. J Appl Toxicol [Internet]. 20191226th ed. 2020;40:706–18. Available from: https://www.ncbi.nlm.nih.gov/pubmed/31877238.
56. Ha DH, Kim SD, Lee J, Kwon HH, Park GH, Yang SH et al. Toxicological evaluation of exosomes derived from human adipose tissue-derived mesenchymal stem/stromal cells. Regul Toxicol Pharmacol [Internet]. 20200522nd ed. 2020;115:104686. Available from: https://www.ncbi.nlm.nih.gov/pubmed/32450131.
57. Ma Y, Liu X, Long Y, Chen Y. Emerging Therapeutic Potential of Mesenchymal Stem Cell-Derived Extracellular Vesicles in Chronic Respiratory Diseases: An Overview of Recent Progress. Front Bioeng Biotechnol [Internet]. 20220225th ed. 2022;10:845042. Available from: https://www.ncbi.nlm.nih.gov/pubmed/35284423.
58. Giri J, Galipeau J. Mesenchymal stromal cell therapeutic potency is dependent upon viability, route of delivery, and immune match. Blood Adv [Internet]. 2020;4:1987–97. Available from: https://www.ncbi.nlm.nih.gov/pubmed/32384543.
59. Brennan FR, Morton LD, Spindeldreher S, Kiessling A, Allenspach R, Hey A et al. Safety and immunotoxicity assessment of immunomodulatory monoclonal antibodies. MAbs [Internet]. 20100523rd ed. 2010;2:233–55. Available from: https://www.ncbi.nlm.nih.gov/pubmed/20421713.
60. McBlane JW. Preclinical safety testing for cell-based products using animals. Biologicals [Internet]. 20150527th ed. 2015;43:425–8. Available from: https://www.ncbi.nlm.nih.gov/pubmed/26026578.
61. Zhu X, Badawi M, Pomeroy S, Sutaria DS, Xie Z, Baek A et al. Comprehensive toxicity and immunogenicity studies reveal minimal effects in mice following sustained dosing of extracellular

vesicles derived from HEK293T cells. J Extracell Vesicles [Internet]. 20170606th ed. 2017;6:1324730. Available from: https://www.ncbi.nlm.nih.gov/pubmed/28717420.

## Supplementary Files

Tables S1 and S2 not available with this version.

## Figures

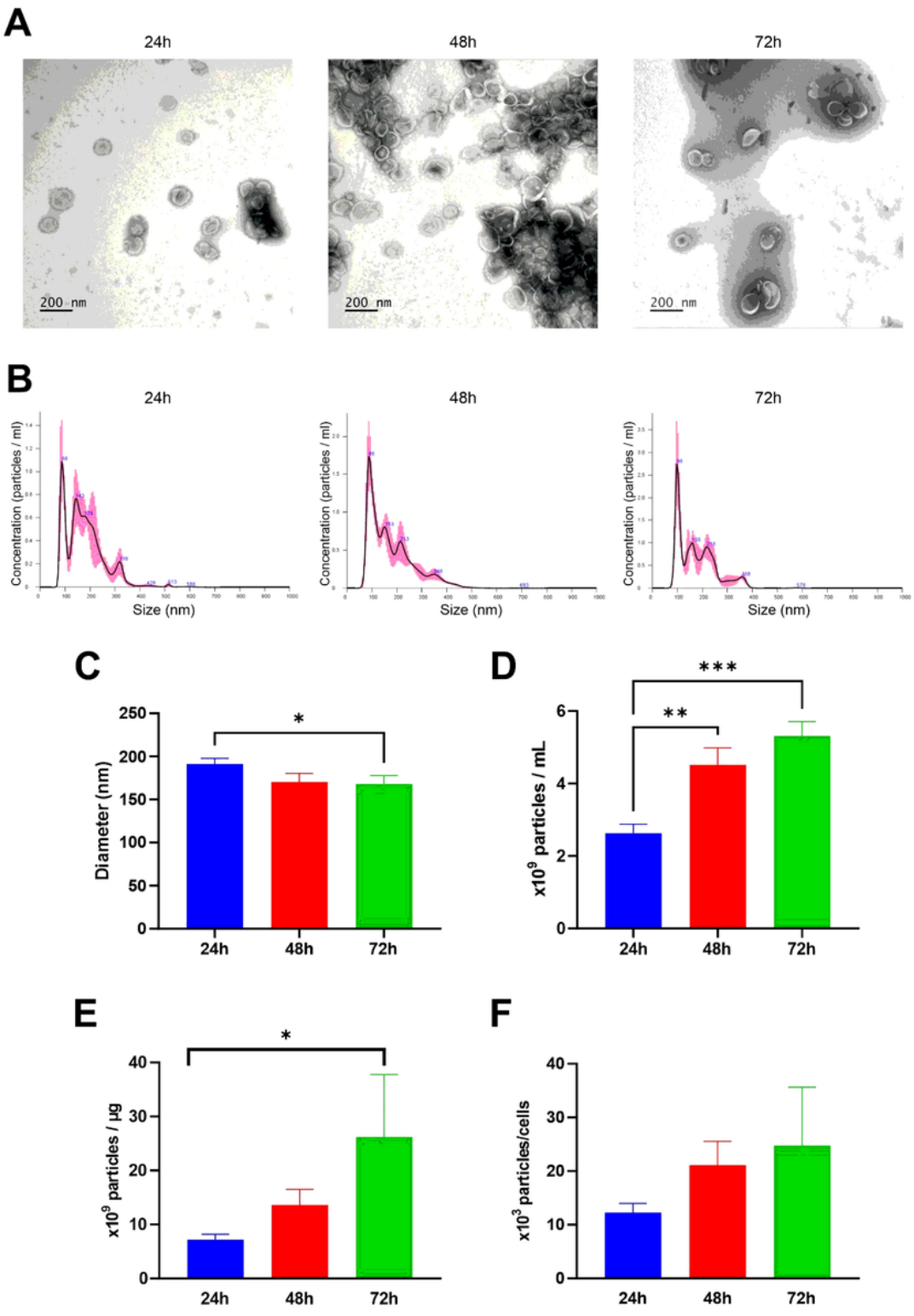


## Figure 1

Characterization of hUCMSC-EVs purified from conditioned medium at different harvest timepoints. **A** Representative images of hUCMSC-EVs observed by transmission electron microscopy. **B** Representative curves of the size distribution and concentration of hUCMSC-EVs by nanoparticle tracking analysis (NTA). **C** Mean diameter of hUCMSC-EVs measured by NTA. **D** Concentration of hUCMSC-EVs measured by NTA. **E** Purity of EVs measured as the ratio between the nanoparticle and protein concentrations. **F**EV

productivity, measured by the ratio between total number of nanoparticles and the number of producer cells at each timepoint. *$P < 0.05$; **$P < 0.01$; ***$P < 0.001$. hUCMSC-EVs, human umbilical cord mesenchymal stromal cell-derived extracellular vesicles.

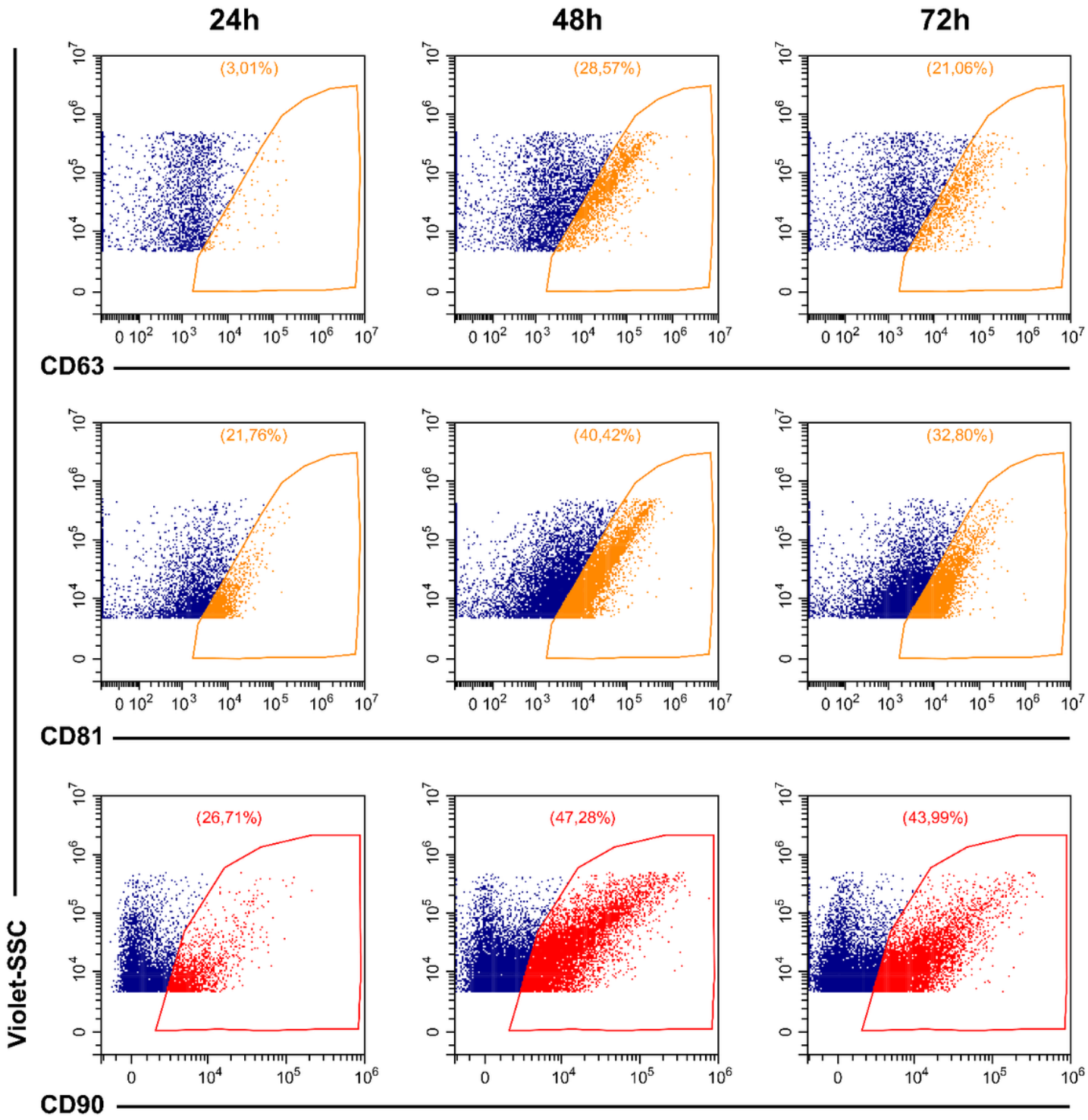


## Figure 2

Immunophenotype of hUCMSC-EVs evaluated by nanoflow. Representative flow cytometry dot plots of hUCMSC-EVs samples stained for the tetraspanins CD63 and CD81, and the mesenchymal stromal cell

marker CD90. hUCMSC-EVs, human umbilical cord mesenchymal stromal cell-derived extracellular vesicles.

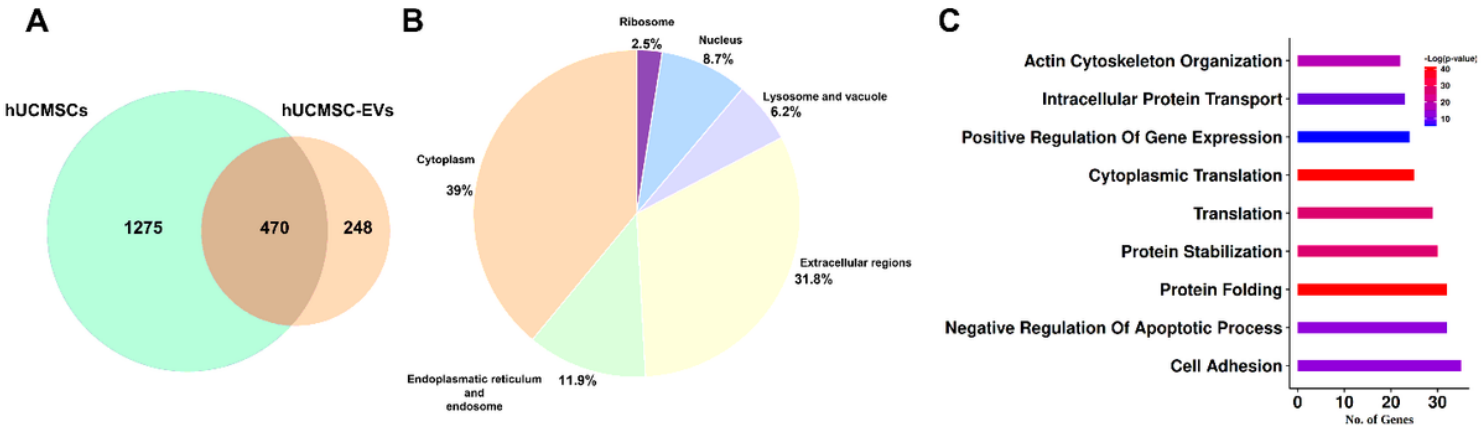


## Figure 3

Protein identification and functional enrichment analysis of hUCMSCs and hUCMSC-EVs. **A** Venn diagram of the proteins detected in hUCMSCs against hUCMSC-EV samples and hUCMSC-EV proteins at different harvesting times (24, 48, and 72 h). **B** Gene Ontology (GO) cellular component of the shared proteins in hUCMSC and hUCMSC-EV samples. The pie chart shows selected significantly enriched categories conducted with SubcellulaRVis (http://phenome.manchester.ac.uk/subcellular/). **C** GO biological process of proteins in common in the hUCMSC and hUCMSC-EV samples. Significantly enriched terms for biological process and cellular components were selected ($P < 0.05$). hUCMSC-EVs, human umbilical cord mesenchymal stromal cell-derived extracellular vesicles.

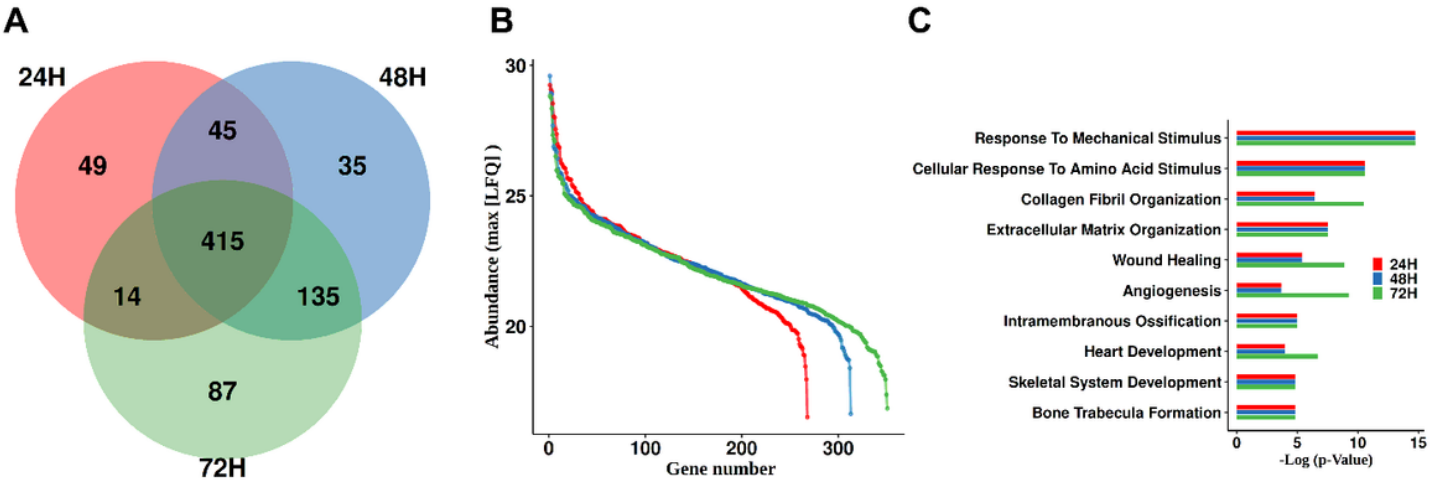


## Figure 4

Bioinformatics analysis of the top 20 most abundant proteins in hUCMSC-EV samples. **A** Venn diagram showing the overlap between hUCMSC-EV samples harvested at different timepoints. **B** Expression–abundance curve of hUCMSC-EVs samples based on label-free quantification. **C**Gene Ontology biological process terms in common displayed by the most abundant proteins found in the 24, 48, and 72h samples of hUCMSC-EVs. The bar represents the significance of terms for each condition (−log(*P* value). hUCMSC-EVs, human umbilical cord mesenchymal stromal cell-derived extracellular vesicles.

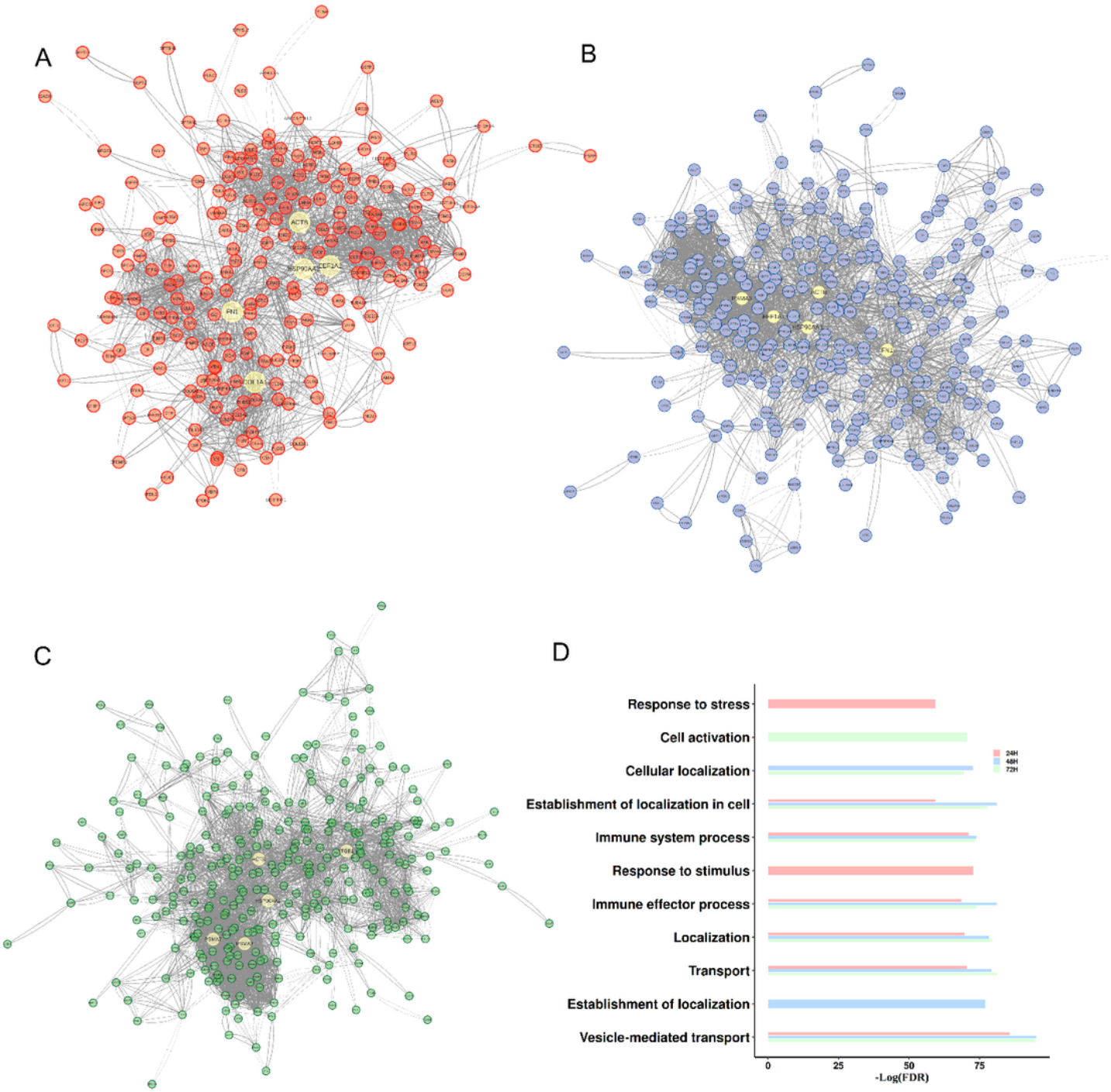

## Figure 5

Protein–protein interaction (PPI) network and hub analysis. **A–C** PPI network at 24 h (red), 48 h (blue), and 72 h (green). The top five hubs are highlighted in yellow. PPI networks were constructed with STRING and only interaction scores >0.7 were kept. **D** Gene Ontology biological processes terms enriched by protein hubs in the PPI network and identified by STRING (https://string-db.org). FDR, false discovery rate.

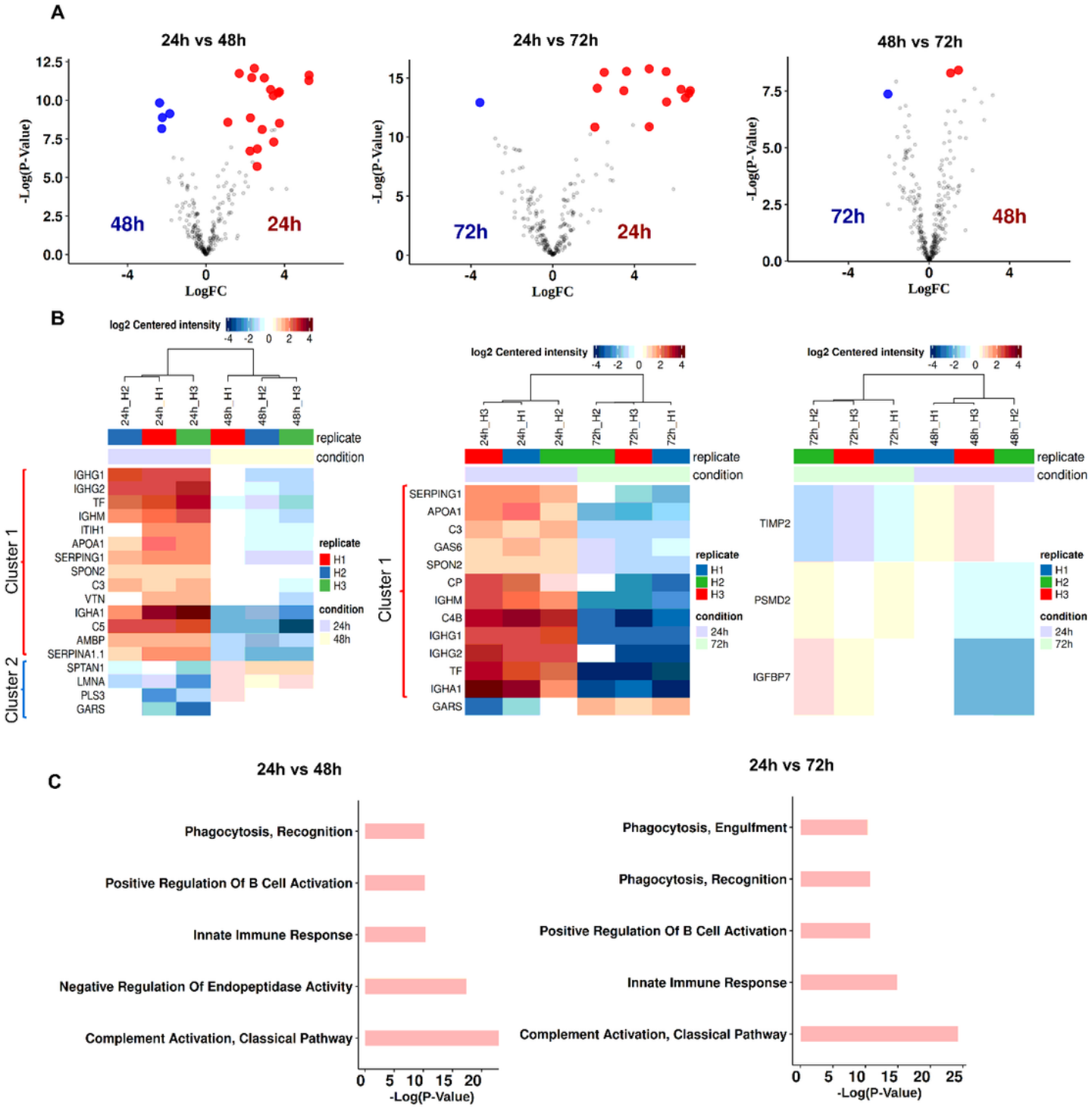

## Figure 6

Analysis of differential expression proteins (DEPs) performed for hUCMSC-EVs conditions. **A** Volcano diagram of DEPs in distinct hUCMSC-EVs harvesting times (24, 48, and 72 h) against pooled hUCMSC-EVs. **B** Heatmap of the protein levels of the DEPs. **C**Biological process enriched terms upregulated at 24 h in contrast with 48 and 72 h. FC, fold change; hUCMSC-EVs, human umbilical cord mesenchymal stromal cell-derived extracellular vesicles.

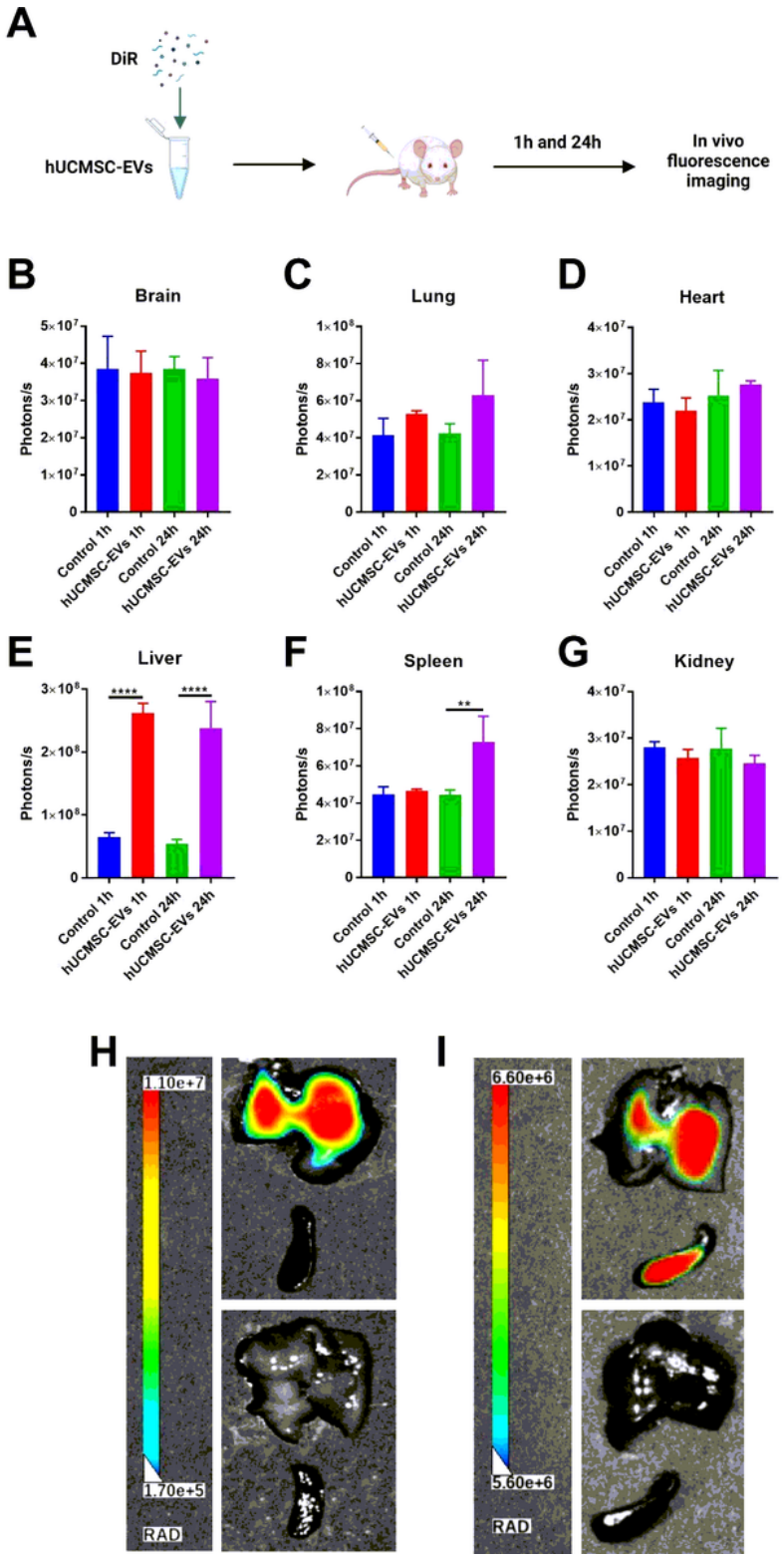

## Figure 7

Biodistribution study of hUCMSC-EVs *in vivo*. **A** Study design for evaluation of the biodistribution of DiR-labeled hUCMSC-EVs in mice after administration via the tail vein. **B–G** Quantification of the fluorescence intensity of different organs. Data are presented as means + standard deviation ($n = 3$). Asterisks indicate significant differences between the groups (**$P < 0.001$; ****$P < 0.0001$; ANOVA followed by Tukey's test). **H, I** Representative *ex vivo* fluorescent images of DiR-labeled hUCMSC-EVs in liver and spleen at 1 h (H) and 24 h (I). DiR, 1,1-dioctadecyl-3,3,3,3-tetramethylindotricarbocyanine iodide; hUCMSC-EVs, human umbilical cord mesenchymal stromal cell-derived extracellular vesicles.

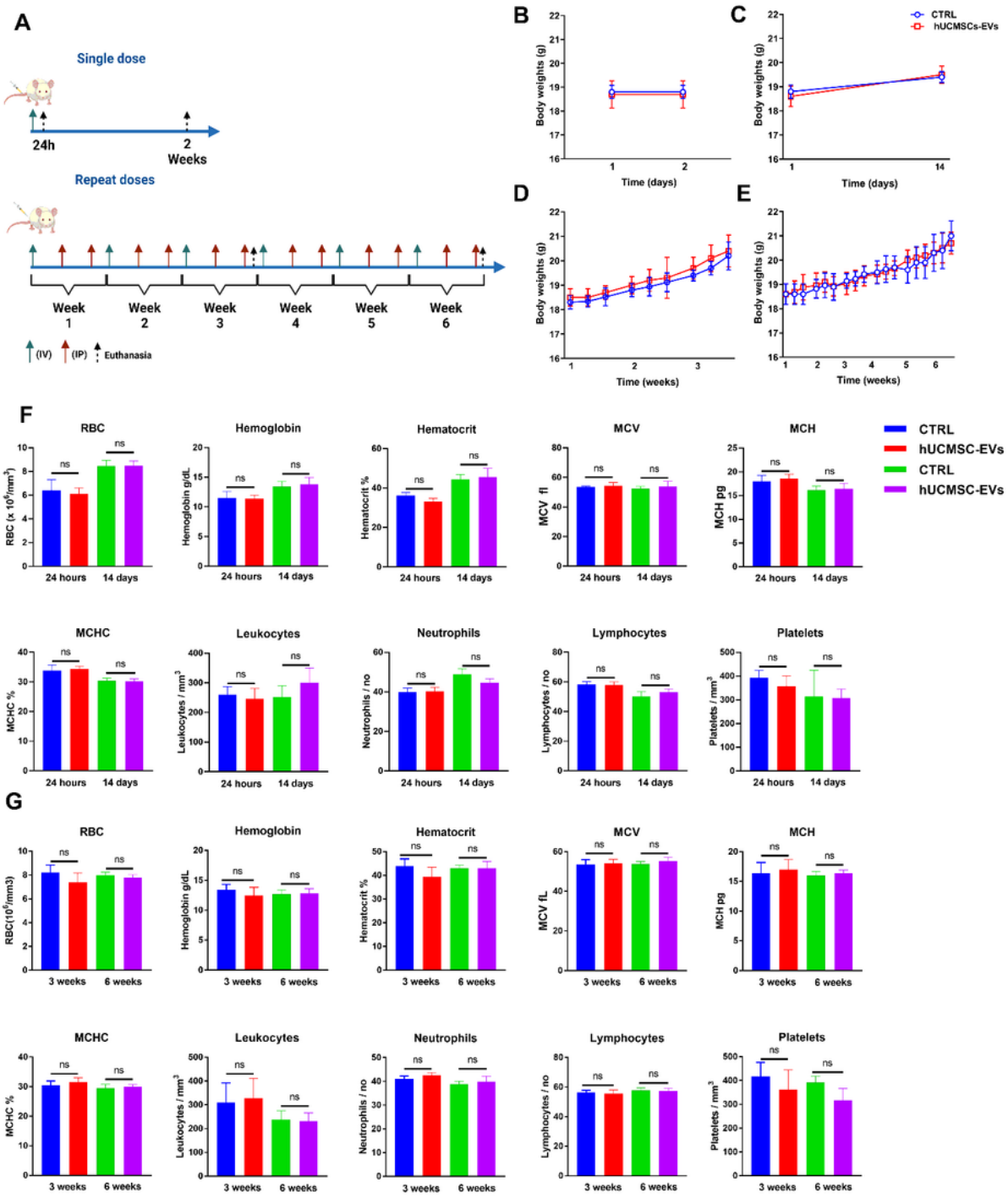


## Figure 8

Effect of hUCMSC-EVs on body weight and hematologic parameters. **A** Time course of the *in vivo* protocol using single and multiple doses. Note intravenous administration (red arrow) and intraperitoneal administration (blue arrow) of hUCMSC-EVs. Animals were euthanized at different times (black arrows). **B–E** Changes in body weight after a single dose (hUCMSC-EVs) at 24 h and 14 days and multiple hUCMSC-EVs doses at 3 and 6 weeks. **F** Hematologic parameters: redblood cell (RBC), mean corpuscular

volume (MCV), mean corpuscular hemoglobin (MCH), and mean corpuscular hemoglobin concentration (MCHC). No statistically significant differences were observed between the groups treated with vehicle or hUCMSC-EVs according to Student's *t* test with *P* values adjusted for multiple comparisons (α = 0.0167 [Bonferroni-adjusted test]). Data are presented as means + standard deviation (*n* = 5). ns, non-significant. CTRL, animals treated with Plasma-Lyte. hUCMSC-EVs, human umbilical cord mesenchymal stromal cell-derived extracellular vesicles.

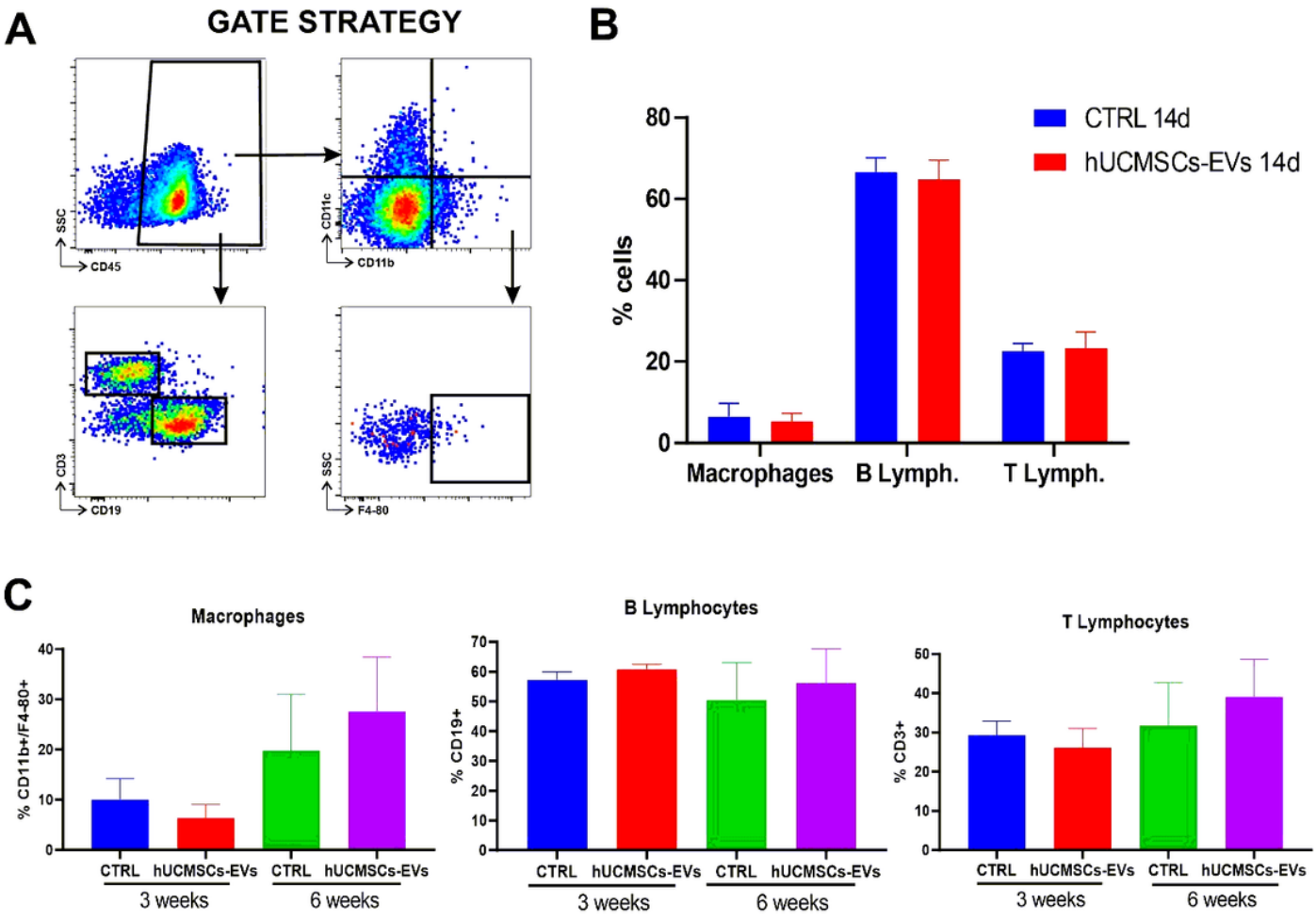


**Figure 9**

Evaluation of immune cell populations in the spleen after single or repeated administration of EVs. **A**Gate strategy for the analysis of immune subpopulations in the spleen. **B**Percentage of macrophages, B and T lymphocytes in spleen samples 14 days after injection of hUCMSC-EVs. **C**Comparisons of macrophages, B and T lymphocytes after 3 and 6 weeks of Plasma-Lyte (CTRL) or injection of hUCMSC-EVs. hUCMSC-EVs, human umbilical cord mesenchymal stromal cell-derived extracellular vesicles.

# Supplementary Files

This is a list of supplementary files associated with this preprint. Click to download.

- CostaFerroetalFigS1Tif.tif
- CostaFerroetalFigS2.tif
- CostaFerroetalFigS3Tif.tif